

Multiethynyl Corannulenes: Synthesis, Structure, and Properties

Yao-Ting Wu,^{†,‡} Davide Bandera,[†] Roman Maag,[†] Anthony Linden,[†]
Kim K. Baldridge,^{*,†} and Jay S. Siegel^{*,†}

*Institute of Organic Chemistry, University of Zurich, Winterthurerstrasse 190,
CH-8057 Zurich, Switzerland, and Department of Chemistry, National Cheng-Kung University,
No.1 Ta-Hsueh Road, Tainan, Taiwan*

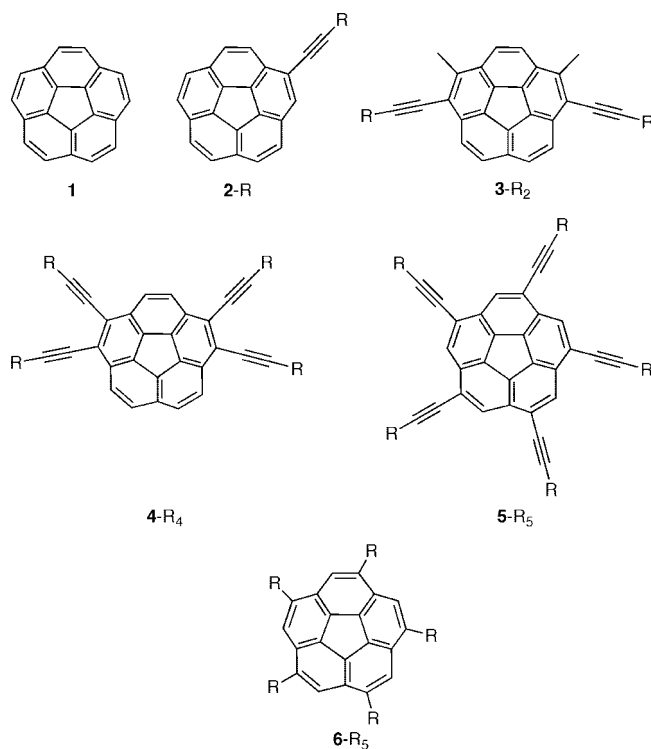
Received March 31, 2008; E-mail: jss@oci.uzh.ch

Abstract: Syntheses, crystal structures, ab initio density functional theory computations, and photophysical properties of 1,6-di-, 1,2,5,6-tetra-, and 1,3,5,7,9-pentaethynyl-substituted corannulenes (classes **3**, **4**, and **5**, respectively) are reported. Classes **3** and **4** were prepared from the corresponding corannulenyl bromides and terminal alkynes in excellent yields (nine examples, with yields of 57–92%) using the Sonogashira reaction. Class **5** was prepared from 1,3,5,7,9-pentachlorocorannulene and trimethylalkynylstannanes using a modification of Nolan's procedure (8 examples, with yields of 45–93%). The molecular packing in crystals of 1,6-diphenylethynyl-2,5-dimethylcorannulene (**3-Ph**₂) displays a polar columnar structure with all of the molecule bowls oriented in the same direction. Similarly, 1,2,5,6-tetrakis(3,5-dimethylphenylethynyl)corannulene [**4-Ar(c)**₅] and 1,3,5,7,9-pentakis(3,5-dimethylphenylethynyl)corannulene [**5-Ar(c)**₅] form columnar structures, but the bowls are oriented in opposing directions. Additionally, the number of attached alkynyl arms is correlated with an increase in bowl depth of the corannulene nucleus. Most of the aryl derivatives displayed high-quantum-efficiency solution luminescence and variable emission wavelengths that were dependent on the nature of the substitution.

Introduction

The shape of corannulene (**1**), a C_{5v}, bowl-shaped fragment of C₆₀¹ and a potential end cap for a single-walled [10,10] carbon nanotube,² evokes the image of an aggregate columnar construction, resembling stacked bowls in a cupboard. Also, the mere fact that **1** is a polynuclear aromatic hydrocarbon with a surface area comparable to that of pyrene suggests that **1** should display exceptional photophysical and electrochemical properties. In contrast to these expectations, **1** is a relatively feeble fluorophore³ and, along with a number of its derivatives, packs in the crystal phase without displaying any columnar order.⁴ The story changes, however, for ethynyl derivatives of **1** (**2–5**; Chart 1), which constitute a particularly efficient set of fluo-

Chart 1. Corannulene and Some of Its Derivatives

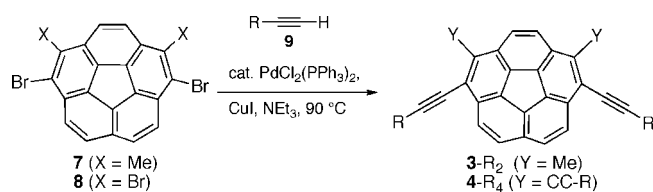


rophores. For example, 1,2-dicorannulenylethyne (**2-Cor**) displays a quantum yield of 0.57 and absorption and emission λ_{max} values similar to those of (phenylethynyl)corannulene (**2-Ph**).⁵

[†] University of Zurich.

[‡] National Cheng-Kung University.

- (1) (a) Wu, Y. T.; Siegel, J. S. *Chem. Rev.* **2006**, *106*, 4843–4867. (b) Sygula, A.; Rabideau, P. W. In *Carbon-Rich Compounds: From Molecules to Materials*; Haley, M., Tykwinski, R., Eds.; Wiley-VCH: Weinheim, Germany, 2006; p 529. (c) Hirsch, A. *Top. Curr. Chem.* **1999**, *199*, 1–65. (d) Scott, L. T. *Pure Appl. Chem.* **1996**, *68*, 291–300. (e) Seiders, T. J.; Siegel, J. S. *Chem. Br.* **1995**, *31*, 307–312.
- (2) (a) Dresselhaus, M. D.; Avouris, P. In *Carbon Nanotubes: Synthesis, Structure, Properties, and Applications*; Dresselhaus, M. D., Dresselhaus, R. S., Avouris, P., Eds.; Springer: Heidelberg, Germany, 2001; p 1. (b) Baldridge, K. K.; Siegel, J. S. *Theor. Chim. Acta.* **1997**, *97*, 67–71.
- (3) (a) Verdick, J. F.; Jankowski, W. A. *Mol. Lumin. Int. Conf.* **1969**, 829–836. (b) Argentine, S. M.; Francis, A. H.; Chen, C.-C.; Lieber, C. M.; Siegel, J. S. *J. Phys. Chem.* **1994**, *98*, 7350–7354. (c) Dey, J.; Will, A. Y.; Agbaria, R. A.; Rabideau, P. W.; Abdourazak, A. H.; Sygula, R.; Warner, I. M. *J. Fluoresc.* **1997**, *7*, 231–236. (d) Mack, J.; Vogel, P.; Jones, D.; Kaval, N.; Sutton, A. *Org. Biomol. Chem.* **2007**, *5*, 2448–2452.

Scheme 1. Synthesis of Di- and Tetraalkynylcorannulenes

The photophysical properties of 5-H₅ and pentaarylcorynnulenes (6-Ar₅; Chart 1)⁶ raise the question of whether it is possible to prepare highly fluorescent materials with columnar arrangements in the solid phase through the use of aryl and alkynyl substituents and a corannulene core.

Results and Discussion

Synthesis. The diethynylcorannulenes 3-R₂ and tetraethynylcorannulenes 4-R₄ were synthesized according to published coupling procedures.⁷ Reaction of 1,6-dibromo-2,5-dimethylcorannulene (7) or 1,2,5,6-tetrabromocorannulene (8) with terminal alkynes under Sonogashira conditions⁸ [catalytic amounts of PdCl₂(PPh₃)₂ and CuI in NEt₃] afforded products in good-to-excellent yields (Scheme 1 and Table 1).

The previously reported preparation of 1,3,5,7,9-pentakis(trimethylsilylethynyl)corannulene (5-TMS₅) from *sym*-pentachlorocorannulene (10) using Eberhard's method with the pincer catalyst 11 required a large excess (50 equiv) of trimethylsilylethyne and high temperature (165 °C).⁶ Recently, improved methods have been reported for Sonogashira-,⁹ Suzuki-,¹⁰ and Stille-type¹¹ couplings involving aryl chlorides. Nolan's protocol is especially attractive.¹² Therefore, a modification of Nolan's protocol was applied for the general preparation of the pentaethynylcorannulenes 5-R₅ from 10 and the corresponding trimethyltin-substituted alkynes (12-R) in reasonable-to-excellent yields (Scheme 2 and Table 1).¹³ In comparison with our previous procedure,⁶ the present synthetic method establishes

Table 1. Synthesis of Class 3, 4, and 5 Multiethynyl-Substituted Corannulenes

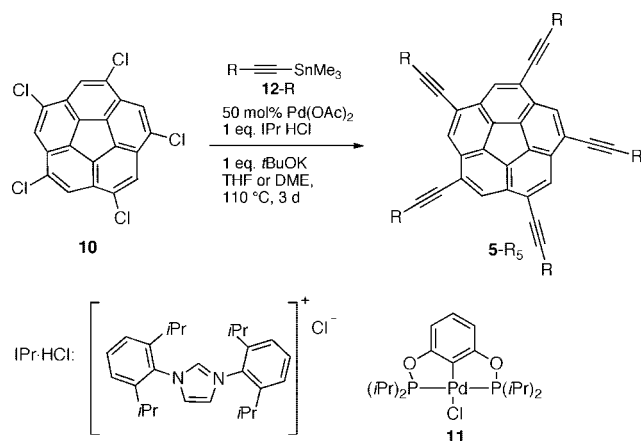
| Entry | Halide | Alkyne | R | Product | Yield (%) |
|-------|--------|----------|-------------------|----------------------|-----------|
| 1 | 7 | 9-TMS | SiMe ₃ | 3-TMS ₂ | 79 |
| 2 | 7 | 9-Ph | Ph | 3-Ph ₂ | 92 |
| 3 | 8 | 9-TMS | SiMe ₃ | 4-TMS ₄ | 85 |
| 4 | 8 | 9-Ph | Ph | 4-Ph ₄ | 86 |
| 5 | 8 | 9-Ar(a) | | 4-Ar(a) ₄ | 83 |
| 6 | 8 | 9-Ar(b) | | 4-Ar(b) ₄ | 55 |
| 7 | 8 | 9-Ar(c) | | 4-Ar(c) ₄ | 82 |
| 8 | 8 | 9-Ar(d) | | 4-Ar(d) ₄ | 91 |
| 9 | 8 | 9-Ar(e) | | 4-Ar(e) ₄ | 85 |
| 10 | 10 | 12-TMS | SiMe ₃ | 5-TMS ₅ | 47 |
| 11 | 10 | 12-Ph | Ph | 5-Ph ₅ | 45 |
| 12 | 10 | 12-Ar(a) | | 5-Ar(a) ₅ | 71 |
| 13 | 10 | 12-Ar(c) | | 5-Ar(c) ₅ | 57 |
| 14 | 10 | 12-Ar(d) | | 5-Ar(d) ₅ | 93 |
| 15 | 10 | 12-Ar(e) | | 5-Ar(e) ₅ | 76 |
| 16 | 10 | 12-Ar(f) | | 5-Ar(f) ₅ | 91 |
| 17 | 10 | 12-Ar(g) | | 5-Ar(g) ₅ | 87 |

milder conditions that require a smaller amount of alkyne and could be used in a large-scale synthesis.

The amount of alkyne required in this procedure appears to depend upon its purity; crude stannanes 12-Ar(a,c-g) required 2 equiv per halide site, whereas 1.5 equiv sufficed for the purer stannylacetylenes 12-TMS and 12-Ph (see the Supporting Information). Commercial tri-*n*-butyl(phenylethynyl)stannane, under the same conditions, did not deliver the desired penta(arylethynyl)corannulene coupling product 5-Ph₅.

The pentachloride 10 is known to be sparingly soluble. After the coupling partners associate, the solubilities of the reaction

- (4) (a) Hanson, J. C.; Nordman, C. E. *Acta Crystallogr.* **1976**, B32, 1147–1153. (b) Petrukhina, M. A.; Andreini, K. W.; Mack, J.; Scott, L. T. *J. Org. Chem.* **2005**, 70, 5713–5716.
- (5) Jones, C. S.; Elliott, E. L.; Siegel, J. S. *Synlett* **2004**, 187–191.
- (6) Grube, G. H.; Elliott, E. L.; Steffens, R. J.; Jones, C. S.; Baldrige, K. K.; Siegel, J. S. *Org. Lett.* **2003**, 5, 713–716.
- (7) (a) Sygula, A.; Rabideau, P. W. *J. Am. Chem. Soc.* **2000**, 122, 6323–6324. (b) Xu, G.; Sygula, A.; Marcinow, Z.; Rabideau, P. W. *Tetrahedron Lett.* **2000**, 41, 9931–9934. (c) Sygula, A.; Xu, G.; Marcinow, Z.; Rabideau, P. W. *Tetrahedron* **2001**, 57, 3637–3644.
- (8) (a) Sonogashira, K.; Tohda, Y.; Hagihara, N. *Tetrahedron Lett.* **1975**, 6, 4467–4470. (b) Sonogashira, K. In *Metal-Catalyzed Cross-Coupling Reactions*; Diederich, F.; Stang, P. J., Eds.; Wiley-VCH: Weinheim, Germany, 1998; pp 203–229. (c) Brandsma, L.; Vasilevsky, S. F.; Verkruysse, H. D. *Application of Transition Metal Catalysts in Organic Synthesis*; Springer: Berlin, 1999; pp 179–225.
- (9) For Sonogashira-type methods, see: (a) Méry, D.; Heuzé, K.; Astruc, D. *Chem. Commun.* **2003**, 1934–1935. (b) Remmele, H.; Köllhofer, A.; Plenio, H. *Organometallics* **2003**, 22, 4098–4103. (c) Köllhofer, A.; Pullmann, T.; Plenio, H. *Angew. Chem., Int. Ed.* **2003**, 42, 1056–1058. (d) Choudary, B. M.; Madhi, S.; Chowdari, N. S.; Kantam, M. L.; Sreedhar, B. *J. Am. Chem. Soc.* **2002**, 124, 14127–14136. (e) Eberhard, M. R.; Wang, Z.; Jensen, C. M. *Chem. Commun.* **2002**, 818–819.
- (10) For Suzuki-type methods, see: Fürstner, A.; Leitner, A. *Synlett* **2001**, 290–292.
- (11) For Stille-type methods, see: (a) Shirakawa, E.; Yamasaki, K.; Hiyama, T. *J. Chem. Soc., Perkin Trans.* **1997**, 1, 2449–2450. For another method, see: (b) Nishihara, Y.; Ikegashira, K.; Hirabayashi, K.; Ando, J.-i.; Mori, A.; Hiyama, T. *J. Org. Chem.* **2000**, 65, 1780–1787.
- (12) Grasa, G. A.; Nolan, S. P. *Org. Lett.* **2001**, 3, 119–122.
- (13) This procedure has been applied in the preparation of 2,3-diethynylcorannulene derivatives. See: Wu, Y. T.; Hayama, T.; Baldrige, K. K.; Linden, A.; Siegel, J. S. *J. Am. Chem. Soc.* **2006**, 128, 6870–6884.

Scheme 2. Synthesis of the Pentaethynyl Corannulene Derivatives **5-R₅**

intermediates increase, enhancing the subsequent coupling reactions. In general, the yields within series **5** tended to be very good overall (70–95%), with single-site coupling efficiencies of >90%. The lower yield (45%) for **5-Ph₅** than for **5-Ar(a,c-f)₅** may reflect the extent to which the addition of side chains imparted increased solubility to the intermediates and products of **5-Ar(a,c-f)₅** during the synthesis reactions.

X-ray Crystallographic Structures of 3-Ph₂, 8, 4-Ar(c)₄, and 5-Ar(c)₅. X-ray-quality crystals of **3-Ph₂**, **8**, **4-Ar(c)₄**, and **5-Ar(c)₅** were obtained and their structures determined as representatives of the corresponding classes (Table 2). All show the characteristic bowl structure of corannulene and internal geometries consistent with their constituent substructures (arene, alkyne, and corannulene). The striking feature in this family of structures is the stacking order. All four compounds adopt essentially columnar packings in either an orthorhombic or a monoclinic unit cell with one particular stacking axis.

Although columnar packing is essentially unobserved in simple corannulene derivatives, the tetrabromide **8** crystallizes in the polar orthorhombic space group *Pna2₁* (Figure 1). Each cell translation along the *c* axis is a step along a column of perfectly stacked bowls (i.e., the normal to the plane of the hub ring is collinear with the stacking axis).¹⁴ Within the stack, the bowls overlap with identical orientations of the hub ring. Neighboring columns are shifted in register but have identical bowl directions; the rotational orientation appears to come from fitting of the bromines. More generally, this kind of unidirectional columnar molecular packing is observed in large non-planar polycyclic compounds, such as circumtrindene (C₃₆H₁₂),¹⁵ trigonal crystals of hemibuckminsterfullerene (C₃₀H₁₂),¹⁶ diindenodeno[1,2,3,4-defg;1',2',3',4'-mnop]chrysene (C₂₆H₁₂),¹⁷ and semibuckminsterfullerene (C₃₀H₁₂).¹⁸

A crystal of **3-Ph₂** was obtained by slow evaporation of the CH₂Cl₂/MeOH solvent mixture at ambient temperature. The

structure (Figure 2) was solved in the polar orthorhombic space group *Pca2₁*, but here the translational element along the *c* axis moves two steps along the column of stacked bowls. The hub rings in each molecular pair are oriented in opposite directions about their centroids. The bowl direction along the stack is the same, save for a distinct tilting of the hub plane with respect to the stacking axis (i.e., the normal to the hub plane forms an angle of 12.2° with the *c* axis). Neighboring columnar stacks have the same bowl direction. The molecular order in the *ab* plane places the body of one molecule next to the arms of the adjacent ones. The arylalkynyl arms fill the voids between corannulenyl units and adopt conformations that optimize arene–arene T interactions (Figure 3).

Because of the low solubilities of **4-Ph₄** and **5-Ph₅** in most common organic solvents (e.g., CH₂Cl₂, toluene, etc.), we could not prepare crystals suitable for X-ray structure analysis. Therefore, more-soluble derivatives having short side chains on the phenyl rings were studied. Crystals of the compounds **4-Ar(c)₄** and **5-Ar(c)₅** were obtained by slow evaporation of the CH₂Cl₂/CHCl₃/MeOH solvent mixture at ambient temperature. Diffraction data for **4-Ar(c)₄** and **5-Ar(c)₅** were recorded at 273 and 260 K, respectively, instead of the usual 160 K because it was found that these crystals crack at the lower temperature.

The structure of **4-Ar(c)₄** (Figure 4) was solved in the space group *Pnma* with one molecule sitting on a special position of crystallographic *C_s* symmetry. After the corannulene core had been modeled, it was found that the unit cell contained two remaining voids, each with a volume of 173 Å³. Difference Fourier maps revealed four unconnected peaks distributed on and about a mirror plane within each void. It was assumed that these voids represented water molecules, i.e., that the formula was C₆₀H₄₂·1.5H₂O. Attempts to include the water molecules in the model did not produce satisfactory results, although it was clear that the sites were only partially occupied. Subsequently, the contribution of the solvent molecules to the intensity data was removed using the SQUEEZE¹⁹ routine of the PLATON²⁰ program.

In the structure of **4-Ar(c)₄**, translation along the *a* axis coincides with moving two steps along the column of stacked bowls. The hub rings in each molecular pair are oriented in opposite directions about their centroids. The bowl direction along the stack is the same, save for a small tilting of the hub plane with respect to the stacking axis (i.e., the normal to the hub plane forms an angle of 4.8° with the *a* axis). Neighboring columnar stacks along the *c* axis have the same bowl direction; adjacent columns along the *c* axis define the columnar channel housing the disordered solvents. These like-pointing columnar stacks define a layer in the *ac* plane. The bowl directions in neighboring planes are antiparallel; the interface between layers fits without any appreciable voids or channels (Figure 4).

The structure of **5-Ar(c)₅** (Figure 5) was solved in the monoclinic space group *P2₁/n*. There are two **5-Ar(c)₅** molecules in the asymmetric unit. Each molecule must sit on a general position because the *C₅* molecular symmetry is incompatible with any space group. The achiral space group indicates that a racemic mixture of left- and right-handed bowls must be present.

In the standard setting of the monoclinic crystal system, the *b* axis is normal to the *ac* plane. Translation along the *b* axis

- (14) Work on modeling of the relative packing of **7**, **8**, and 1,2,5,6-tetramethylcorannulene is ongoing; Wu, Y. T.; Maag, R.; Potier, Y.; Ciurash, J. G.; Baldridge, K. K.; Hardcastle, K. I.; Linden, A.; Gavezzotti, A.; Siegel, J. S. Unpublished results, 2008.
- (15) Forkey, D. M.; Attar, S.; Noll, B. C.; Koerner, R.; Olmstead, M. M.; Balch, A. L. *J. Am. Chem. Soc.* **1997**, *119*, 5766–5767.
- (16) Petrukhina, M. A.; Andreini, K. W.; Peng, L.; Scott, L. T. *Angew. Chem., Int. Ed.* **2004**, *43*, 5477–5481.
- (17) Bronstein, H. E.; Choi, N.; Scott, L. T. *J. Am. Chem. Soc.* **2002**, *124*, 8870–8875.
- (18) Sygula, A.; Marcinow, Z.; Fronczek, F. R.; Guzei, I.; Rabideau, P. W. *Chem. Commun.* **2000**, 2439–2440.

(19) van der Sluis, P.; Spek, A. L. *Acta Crystallogr.* **1990**, *A46*, 194–201.

(20) Spek, A. L. PLATON, Program for the Analysis of Molecular Geometry; University of Utrecht: Utrecht, The Netherlands, 2005.

Table 2. Crystal Structure Data for the Corannulene Derivatives **3-Ph₂**, **8**, **4-Ar(c)₄**, and **5-Ar(c)₅**

3-Ph₂

8

4-Ar(c)₄

5-Ar(c)₅

| | 3-Ph ₂ | 8 | 4-Ar(c) ₄ | 5-Ar(c) ₅ |
|----------------------------|---------------------------------------|--|--|--|
| formula | C ₃₈ H ₂₂ | C ₂₀ H ₆ Br ₄ | C ₆₀ H ₄₅ O _{1.5} | C ₇₀ H ₅₀ |
| molecular weight | 478.59 | 565.88 | 790.01 | 891.16 |
| solvent | CH ₂ Cl ₂ /MeOH | toluene | CH ₂ Cl ₂ /CHCl ₃ /MeOH | CH ₂ Cl ₂ /CHCl ₃ /MeOH |
| <i>T</i> (K) | 160(1) | 160(1) | 273(1) | 260(1) |
| crystal system | orthorhombic | orthorhombic | orthorhombic | monoclinic |
| space group | <i>Pca</i> 2 ₁ | <i>Pna</i> 2 ₁ | <i>Pnma</i> | <i>P</i> 2 ₁ / <i>n</i> |
| <i>Z</i> | 4 | 4 | 4 | 8 |
| <i>a</i> (Å) | 15.4564(6) | 17.8356(5) | 7.4846(5) | 33.414(1) |
| <i>b</i> (Å) | 22.190(1) | 22.9372(7) | 43.341(3) | 7.8392(3) |
| <i>c</i> (Å) | 7.4161(2) | 3.8032(1) | 13.684(1) | 41.096(2) |
| β (deg) | 90 | 90 | 90 | 109.8771(8) |
| <i>V</i> (Å ³) | 2543.6(2) | 1555.88(8) | 4438.9(5) | 10123.5(7) |

coincides with moving two steps along the column of stacked bowls. The hub rings of each molecular pair are oriented in opposite directions about their centroids. The pairs have the same handedness, and this combines with the opposite orientations of the hub rings to place their arms in a staggered relationship to one another. The bowl direction along the stack is the same, save for a small tilting of the hub plane with respect to the stacking axis (i.e., the normal to the hub plane forms an angle of 6.6° with the *b* axis). Neighboring columnar stacks along the *a* axis have the same bowl direction, whereas those along the *c*-axis have antiparallel bowl directions. The arms of

the aggregated columns embrace, forming a space-filled network with no channels or voids (Figure 5).

All four structures establish that columnar stacking is attainable in substituted corannulenes. These observations reopen the question of controlled stacking in mixtures of arylalkynyl-corannulenes and their perfluoroarylalkynyl analogues. The issues with respect to series **5** would involve control of the stacking order, rotational orientation, bowl direction, and chirality of the individual component bowls (Figure 6).

Molecular Geometries of 3-Ph₂, 8, 4-Ar(c)₄, and 5-Ar(c)₅. The molecular geometry of a corannulene derivative contains three

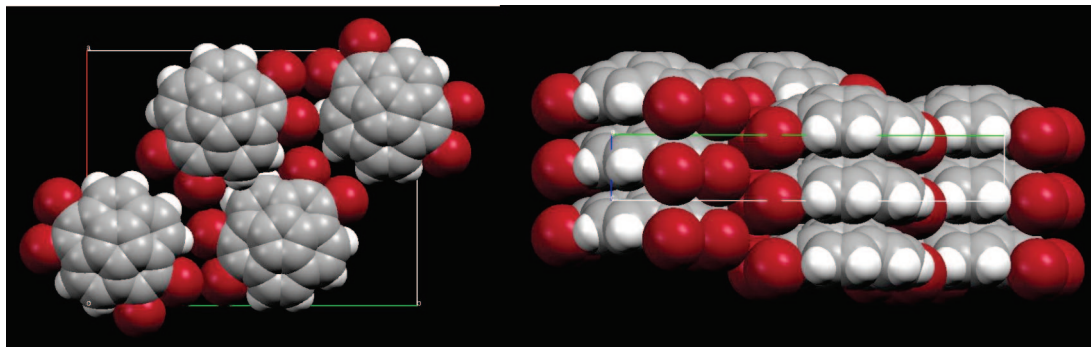


Figure 1. Columnar packing in the crystal structure of **8**.

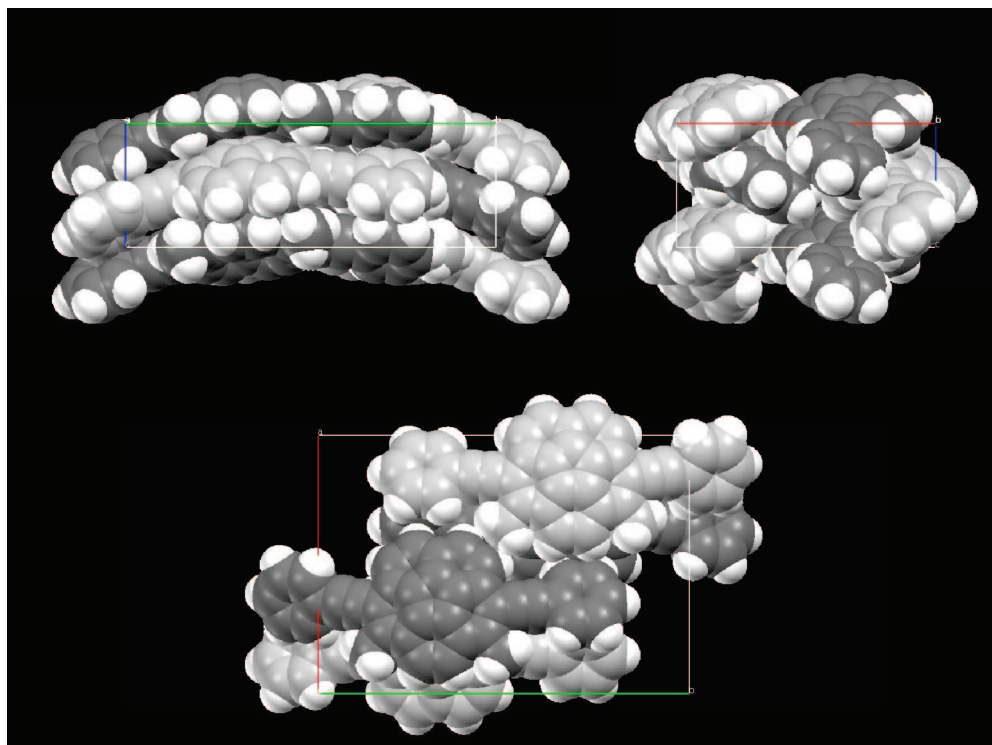


Figure 2. Crystal packing in **3-Ph₂** along the (top left) *a*, (top right) *b*, and (bottom) *c* axes.

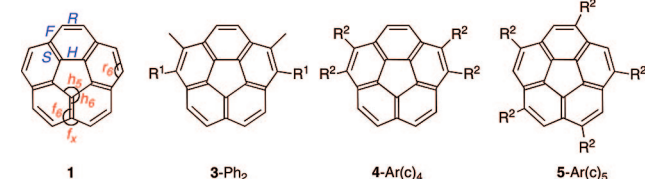
atom types [hub (H), spoke (S), and rim (R)] that are connected by four core bond types [H, S, flank (F), and R] and about which five descriptive angles [five-ring hub (h_5), six-ring hub (h_6), six-ring flank (f_6), exo flank (f_x), and six-ring rim (r_6)] are defined. The typical structural motif follows the pattern of a [5]radialene with five rim double bonds (H and F lengths > S and R lengths) and angles determined by symmetry and atom pyramidalities or bowl depth ($h_5 = 108^\circ$; $h_6 = 120\text{--}126^\circ$; $f_6 = 115^\circ$, $f_x = 130^\circ$; $r_6 \geq 120^\circ$). The bulk of the pyramidal character is seen in the hub atoms, as gauged by π -orbital axis vector (POAV) angles²¹ (flat = 0; corannulene = 8° ; C_{60} = 13°). The bowl depth is typically measured as the distance between the rim and hub

mean planes or as the average of the distances of the hub atoms from the rim mean plane (flat = 0 Å; corannulene = 0.87 Å; C_{60} = 1.1 Å). This set of parameters forms a useful taxonomic set for the characters of corannulene bowl fragments ranging from flat to fullerene (nanotube cap).

All three of the arylalkynylcorannulenes **3-Ph₂**, **4-Ar(c)₄**, and **5-Ar(c)₅** follow the standard geometry in their core fragments (Table 3). Correlative trends involving the H_6 angle, bowl depth, and POAV_{hub} angle can be observed. The bowl depth is positively correlated with the POAV_{hub} angle and negatively correlated with the H_6 angle, as would be expected if the hub atoms are the principal sites of out-of-plane distortion. Specific comparison reveals bowl depths of 0.846(7), 0.884(8), and 0.936(5) Å for **3-Ph₂**, **4-Ar(c)₄**, and **5-Ar(c)₅**, respectively, and corresponding POAV_{hub} and h_6 angles of 8.00(14), 8.2(3), and 8.7(2) $^\circ$ and 123.1(2), 122.9(3), and 122.6(12) $^\circ$, respectively.

Alkyl rim substituents on corannulene flatten the bowl and decrease the inversion barrier.²² In contrast, for arylalkynyl substituents, the crystal structure analyses of **3-Ph₂**, **4-Ar(c)₄**, and **5-Ar(c)₅** showed that the bowl depth increases with the number of attached alkynyl groups. It is striking that **5-Ar(c)₅**

- (21) (a) Haddon, R. C. *Science* **1993**, *261*, 1545–1550. (b) Haddon, R. C. *J. Am. Chem. Soc.* **1990**, *112*, 3385–3389. (c) Haddon, R. C. *Acc. Chem. Res.* **1988**, *21*, 243–249. (d) Haddon, R. C.; Scott, L. T. *Pure Appl. Chem.* **1986**, *58*, 137–142.
- (22) The bowl depths and inversion barriers for 1,6-dimethylcorannulene (0.866 Å and 9.0 kcal/mol, respectively), 2,5-dimethylcorannulene (0.865 Å and 9.0 kcal/mol), and 1,3,5,7,9-pentamethylcorannulene (0.850 Å and 8.7 kcal/mol) are smaller than those for corannulene (calcd 0.877 Å and 9.2 kcal/mol; exptl 11.5 kcal/mol). For details, see: Seiders, T. J.; Baldrige, K. K.; Grube, G. H.; Siegel, J. S. *J. Am. Chem. Soc.* **2001**, *123*, 517–525.

Table 3. Bond Distances (Å), Angles (deg), Bowl Depths (Å), and Hub POAV Angles (deg) for **1**, **3-Ph**₂, **4-Ar(c)**₄, and **5-Ar(c)**₅


| | 1 ^a | | 3-Ph ₂ | | 4-Ar(c) ₄ | | 5-Ar(c) ₅ | |
|--|-----------------------|--------------------|--------------------------|--------------------|-----------------------------|--------------------|-----------------------------|--------------------|
| | exptl | calcd ^c | exptl | calcd ^c | exptl | calcd ^c | exptl | calcd ^c |
| bond lengths ^{b,d} | | | | | | | | |
| R | 1.380(2) | 1.392 [1.384] | 1.388(13) | 1.397 [1.388] | 1.387(19) | 1.405 [1.393] | 1.390(5) | 1.409 [1.396] |
| F | 1.444(2) | 1.450 [1.448] | 1.449(10) | 1.445 [1.449] | 1.450(7) | 1.453 [1.449] | 1.435(7) | 1.439 [1.439] |
| H | 1.414(2) | 1.419 [1.419] | 1.410(6) | 1.418 [1.417] | 1.415(8) | 1.418 [1.417] | 1.409(5) | 1.418 [1.417] |
| S | 1.378(2) | 1.387 [1.380] | 1.374(7) | 1.386 [1.379] | 1.372(5) | 1.385 [1.379] | 1.390(7) | 1.386 [1.379] |
| angles ^{b,d} | | | | | | | | |
| h ₅ | 108.0(1) | 108.0 [108.0] | 108.0(2) | 108.0 [108.0] | 108.0(4) | 108.0 [108.0] | 108.0(4) | 108.0 [108.0] |
| h ₆ | 122.9(2) | 123.0 [122.9] | 123.1(2) | 123.0 [122.9] | 122.9(3) | 123.1 [122.9] | 122.6(12) | 123.1 [122.8] |
| f ₆ | 114.3(2) | 114.3 [114.5] | 114.4(7) | 114.4 [114.6] | 114.8(5) | 114.6 [114.8] | 114.8(6) | 114.6 [114.9] |
| f ₈ | 130.1(4) | 130.1 [129.8] | 130.0(5) | 130.1 [129.6] | 129.0(6) | 129.8 [129.1] | 128.8(6) | 129.7 [129.0] |
| r ₆ | 122.0(2) | 122.0 [122.0] | 121.8(8) | 121.9 [121.8] | 121.6(6) | 121.6 [121.6] | 121.9(8) | 121.6 [121.5] |
| bowl depth | 0.875(2) | 0.873 [0.887] | 0.846(7) | 0.861 [0.879] | 0.884(8) | 0.848 [0.888] | 0.936(5) | 0.853 [0.892] |
| POAV _{hub} angle ^e | 8.3(2) | 8.2 [8.3] | 8.00(14) | 8.1 [8.3] | 8.2(3) | 8.0 [8.4] | 8.7(2) | 8.0 [8.4] |

^a Data taken from ref 4a,b. ^b All values are averages over bond type. Underlined values identify closer agreement between experiment and theory. ^c B3LYP/cc-pVDZ [M06-2X/cc-pVDZ]. ^d Bond types: H = Hub; S = Spoke; F = Flank; R = Rim. Angle types: h₅ = five-ring hub; h₆ = six-ring hub; f₆ = six-ring flank; f₈ = exo flank; r₆ = six-ring rim. ^e Pyramidity measure; see ref 21.

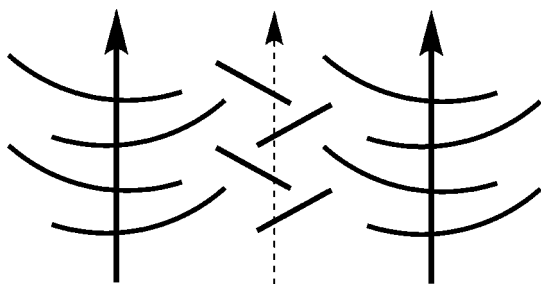


Figure 3. Orientation of corannulene units and adjacent arylalkynyl arms in the stacking of **3-Ph**₂. Arene–arene T interactions are prevalent. Arrows define the stacking axes (bold for foreground, dashed for background). Curves represent corannulene, and bars represent arylalkynyl arms.

has a deeper bowl [0.936(5) Å] and is more pyramidal at the hub carbons [8.7(2)°] than the parent corannulene [0.875(2) Å, 8.3(2)°], which would suggest that the bowl-inversion process would be slower for such derivatives. A general investigation of *sym*-penta-X-corannulenes could reveal whether this effect is general for electronegative substituents.

Having a well-defined set of parameters and a chemically reasonable trend makes this set of compounds a good testing ground for computational methods. Recent advances in density functional theory (DFT) treatments, and in particular, incorporation of dispersive effects, are in need of scrutiny. Here, results obtained with the cc-pVDZ basis set using both the classical DFT functional B3LYP, which has been broadly employed in previous investigations of other corannulene-based structures and coupled with second-order Moller-Plesset perturbation theory (MP2) for the accurate determination of bowl dynamics, and the new functional M06-2X are compared to the current X-ray crystallographically derived data.

Examination of the B3LYP/cc-pVDZ and M06-2X/cc-pVDZ geometries in direct comparison to the experimental data shows remarkable agreement for the average bond angles: corresponding values computed using the two methods never deviated from each other or the experimental data by more than 0.9°. In the

case of bond lengths, all of the values predicted using M06-2X fell within 0.01 Å of the experimental values, whereas B3LYP overestimated all of the rim and spoke bond lengths across the series by >0.01 Å, except for the spoke of **5-Ar(c)**₅. Of these two methods, only M06-2X predicted the positive correlation between bowl depth and POAV_{hub} that was observed experimentally, although the calculated effect was much less dramatic (Table 3).

Photophysical Properties. Now that the possibility of stacking corannulene derivatives in the solid state has been addressed, the second point, related to producing enhanced photophysical properties, remains. Previously, the photophysical properties of **1**, **2-TMS**, and **2-Ph** were examined in cyclohexane, and these compounds were found to be modest fluorophores. The present measurements offer a more extensive database of the photophysical properties of classes **2**, **3**, **4**, and **5** in dichloromethane (Table 4) that can be employed to elucidate the effects of arylalkynyl substitution as well as general aryl effects.

For the purpose of discussion, the present classes of molecules are viewed as having a central corannulene fragment and a perturbing substituent field. The principal subsymmetries of *C*_{5v} are a *C*₅ proper rotation axis and five mirror planes (*σ*) individually representing *C*_s symmetry. The symmetry perturbations due to arylalkyne substitution for classes **2**, **3**, **4**, and **5** are *C*₁, *C*_s, *C*_s, and *C*₅, respectively. The nodal structures and symmetries of the frontier orbitals manifest the substituent effects.

The parent corannulene is *C*_{5v}-symmetric and has a quadruply degenerate HOMO (2 × *E*₁, 2 × *E*₂; see Figure 7); the highest occupied orbital of A-type symmetry is the HOMO-4 orbital. The virtual-orbital space begins with a doubly degenerate set (*E*₂) followed by an orbital of A-type symmetry. The principal transitions are π-to-π*, with several transitions that are cryptic because of small extinction coefficients.

In the case of class **5**, where the *C*₅ symmetry allows for effective interaction between the substituent field and the orbital of A symmetry in the corannulene core, the resultant orbital of

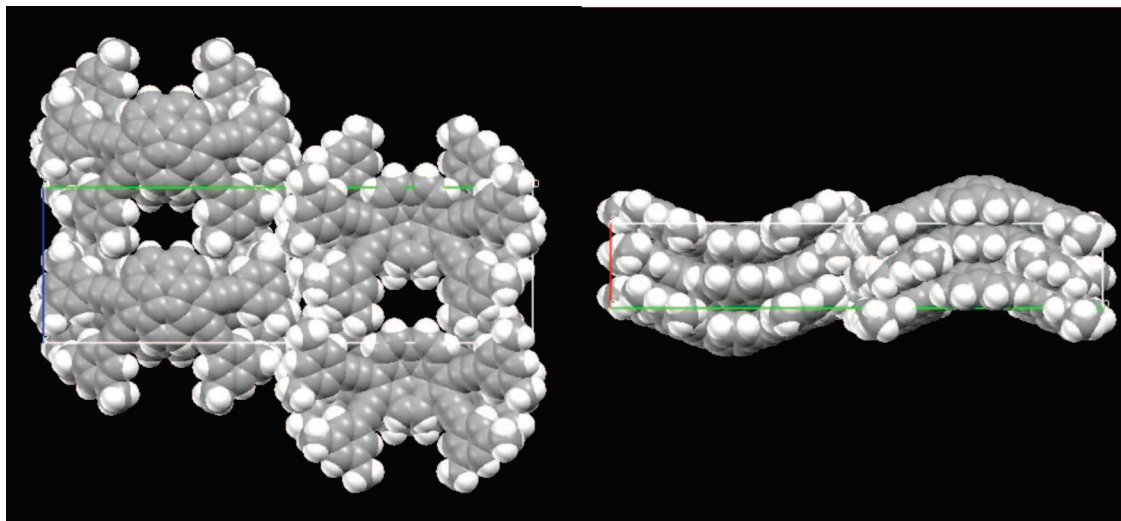


Figure 4. Crystal packing in **4-Ar(c)**₄ along the (left) *a* and (right) *c* axes.

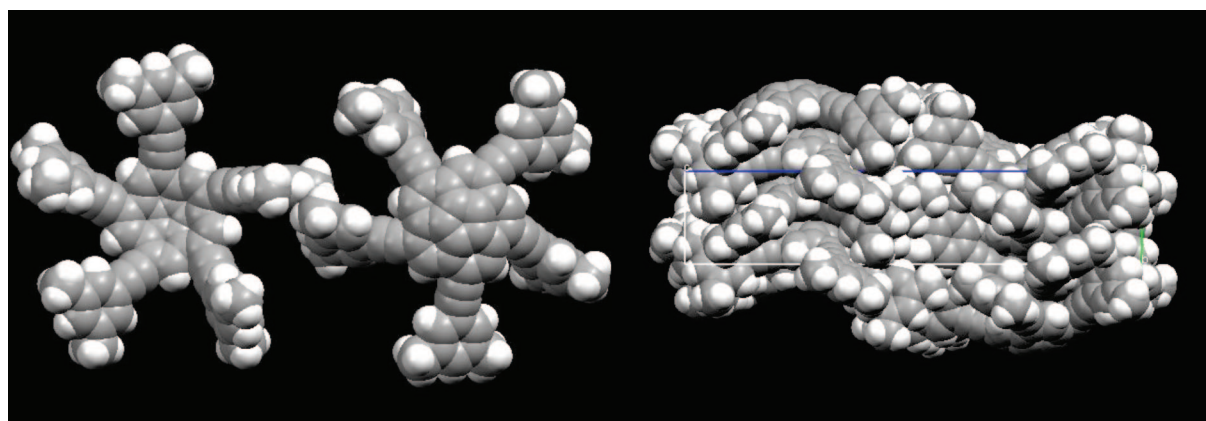


Figure 5. Crystal packing in **5-Ar(c)**₅: (left) the two-molecule asymmetric unit; (right) view along the *c* axis.

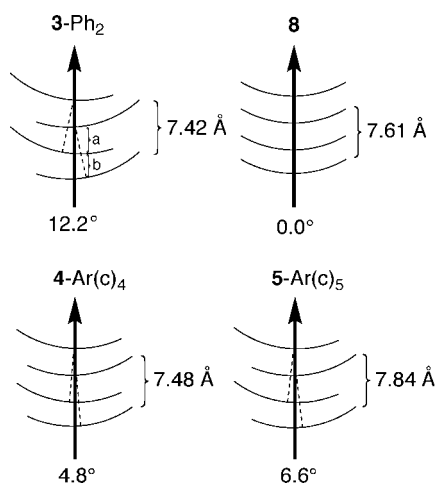


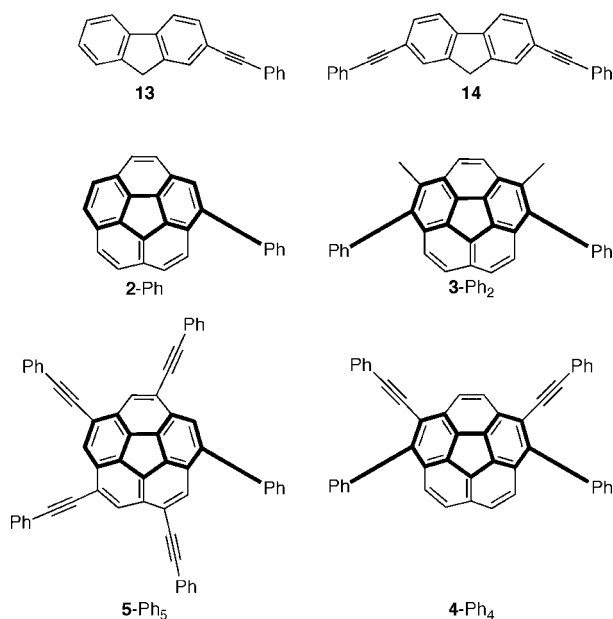
Figure 6. Comparison of the stacking order parameters for **3-Ph**₂, **8**, **4-Ar(c)**₄, and **5-Ar(c)**₅. Arrows define the stacking axes, and curves represent corannulene fragments.

A symmetry (HOMO-4) represents an antibonding interaction between the core and the field. The two sets of E-type orbitals (i.e., 4 orbitals total) remain essentially degenerate, forming a complex HOMO-to-HOMO-3 orbital manifold. The computations predicted a manifold of π -to- π^* transitions among degenerate HOMO and LUMO levels that have essentially no

transition moment because of symmetry. The first transition with any significant absorptivity appears at 360 nm [358 nm ($\log \epsilon$ 5.0) exptl]. As is observed in benzene, the frontier orbitals with mutually exclusive nodal structures lead to poor Franck–Condon factors for HOMO-to-LUMO transitions.

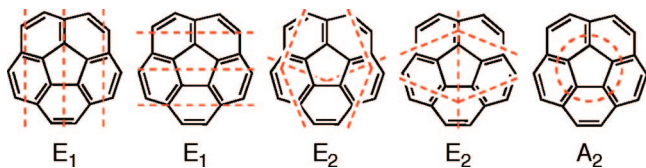
For classes **3** and **4**, the intersection of the C_s symmetry of the field and the C_{5v} symmetry of the core results in a molecular symmetry of C_s . Although the orbitals are formally of the A' and A'' types, their nodal structures and relative energies indicate their origins. In class **3**, the quasi-diametrically opposed substituents at the 1 and 6 positions on corannulene fall essentially along the nodal planes of two of the E-type orbitals (Figure 8). As a result, there is no core-to-field perturbation, and these orbitals remain at essentially their “non-interacting” energies. In contrast, the other two E-type orbitals are well-suited spatially and by symmetry to interact with the field orbitals, and HOMO and HOMO-1 are the resultant antibonding combinations of this core-to-field interaction. Thus, even though the four orbitals should be energetically separated according to symmetry arguments, the HOMO-2 and HOMO-3 orbitals are effectively degenerate. The longest-wavelength principal absorption (377 nm exptl) is predicted to be a strong HOMO-to-LUMO transition with a calculated wavelength of 368 or 396 nm (depending on the method used; see Table 4).

The four substituents in class **4** set up a symmetry field similar to that in class **3** but present a different spatial distribution of

Table 4. Photophysical Properties of Multiethynyl-Substituted Corannulene Derivatives^a

| entry | compound | λ_a [nm] ($\log \epsilon$ [$M^{-1} \text{ cm}^{-1}$]) | λ_{calcd}^c | λ_f (nm) | Φ_f | τ (ns) |
|-------|----------------------------|--|--|------------------------|----------|-------------|
| 1 | 1 | 320 ^{sh} (4.0), 288 (4.7), 254 (5.0) | | 423 | 0.03 | 7.3 |
| 2 | 2-TMS | 297 (4.6) | | 435 | 0.07 | 8.0 |
| 3 | 2-Ph | 400 ^{sh} , 363–345 (4.1) , 298 ^{br} (4.7) | 340 , 313, 272 [375 , 315, 292] | 434, 415 | 0.20 | 6.6 |
| 4 | 7 | 292 (4.8), 259 ^{br} (5.0) | | 446, 426 | 0.029 | 7.8 |
| 5 | 3-TMS₂ | 416 ^{sh} (3.3), 371 ^{sh} (4.0), 353 ^{sh} (4.1), 307 (4.6) | | 455, 442 ^{sh} | 0.25 | 5.5 |
| 6 | 3-Ph₂ | 425 ^{sh} , 378–359 (4.4) , 320 ^{sh} , 298 (4.6) | 368 , 315, 275 [396 , 347, 313] | 469, 446 | 0.75 | 4.8 |
| 7 | 4-TMS₄ | 331 (4.8) | | 475, 449 | 0.17 | 11.1 |
| 8 | 4-Ph₄ | 450 ^{weak} , 400^{sh}, 356 (4.9) , 305 (4.9), 288 | 399 , 363 , 328, 314, 286 [429, 399 , 352/344 , 321, 285] ^d | 500, 473 | 0.83 | 10.3 |
| 9 | 4-Ar(a)₄ | 370 (4.8) | | 529 | 0.67 | 7.9 |
| 10 | 4-Ar(b)₄ | 458 ^{sh} (3.8), 361 (4.9), 332 (4.9), 312 ^{sh} (4.9) | | 504, 476 | 0.58 | 9.1 |
| 11 | 4-Ar(d)₄ | 381 (4.9), 361 ^{sh} (4.9), 319 ^{sh} (4.9) | | 506 | 0.71 | 6.5 |
| 12 | 4-Ar(e)₄ | 382 (4.9), 331 (4.9) | | 527, 501 | 0.73 | 6.0 |
| 13 | 5-TMS₅ | 339 (4.7), 303 (4.9) | | 468, 452 | 0.05 | 9.5 |
| 14 | 5-Ph₅ | 358 (5.0) , 324 (5.0) , 284 (4.9) | 365 , 332 , 286 [360 , 348/325 , 290] | 485, 465 | 0.12 | 10.5 |
| 15 | 5-Ar(a)₅ | 376 (5.0), 332 ^{sh} (4.9) | | 542 | 0.37 | 8.4 |
| 16 | 5-Ar(d)₅ | 383 (5.0), 354 ^{sh} (4.9), 345 (5.0), 306 (5.0), 287 (5.0) | | 503 | 0.24 | 5.8 |
| 17 | 5-Ar(e)₅ | 385 (5.0), 345 ^{sh} (5.0), 321 (5.0) | | 499, 485 | 0.44 | 8.9 |
| 18 | 5-Ar(f)₅ | 364 (4.9), 328 (4.9) | | 491, 465 | 0.16 | 11.0 |
| 19 | 5-Ar(g)₅ | 374 (5.0), 334 (4.9), 322 ^{sh} (4.8) | | 498, 479 | 0.26 | 10.2 |
| 20 | 13 | 335 (4.6), 319 (4.6) | 305 [346] | 357, 340 | 0.89 | 0.75 |
| 21 | 14 | 363 ^{sh} (4.7), 346 (4.9), 317 ^{sh} (4.6) | 333 [377, 333] | 391, 370 | 0.94 | 0.65 |
| 22 | 14^b | 362 ^{sh} , 347 (4.9) | | 387, 368 | 1 | 0.67 |

^a All measurements were for samples in degassed dichloromethane. For compounds **3-R₂**, **4-R₄** and **5-R₅**, only absorption bands with $\lambda_a > 300$ nm are given. The excitation wavelength was 306 nm. Quantum yields are relative to 9,10-diphenylanthracene ($\Phi_f = 0.95$) in ethanol. Bold values correspond to those used for comparison of experiment and computation. ^b Data from ref 23; experiments were performed in dioxane. ^c M06-2X/6-311+G(d,p)//M06-2X/cc-pVDZ [ZINDO//M06-2x/cc-pVDZ].

**Figure 7.** Nodal planes for the degenerate orbitals HOMO to HOMO-3 and for the HOMO-4 orbital (A_2 symmetry) in corannulene.

orbital densities and phases. Interaction of the core with all of the E-type orbitals is possible and gives HOMO through HOMO-3 as the resultant antibonding core-to-field interactions (Figure 9). Unlike the ones in **3-Ph₂**, these four orbitals are energetically separated in practice as well as by symmetry arguments. The longest-wavelength principal absorption (400

nm exptl) is predicted to be a HOMO-to-LUMO transition with a calculated wavelength of 363 or 399 nm (Table 4).

The trends in the absorption wavelengths can also be qualitatively rationalized using this picture. The longer-wavelength absorptions for class **4** compared to class **3** come from stronger interactions between filled field and core orbitals (to give the HOMO) and between unfilled field and core orbitals (to give the LUMO). Stronger antibonding and bonding interactions, respectively, between the core and the field lead to higher-lying HOMOs and lower-lying LUMOs. The longer-wavelength absorptions for class **5** are seen computationally but with nominal transition probabilities, which is reflected by the fact that these transitions are experimentally cryptic. The first experimentally observed transition in **5-Ph₅** is at 358 nm, which corresponds to a HOMO-to-LUMO manifold transition with a calculated wavelength of 365 or 360 nm (Table 4).

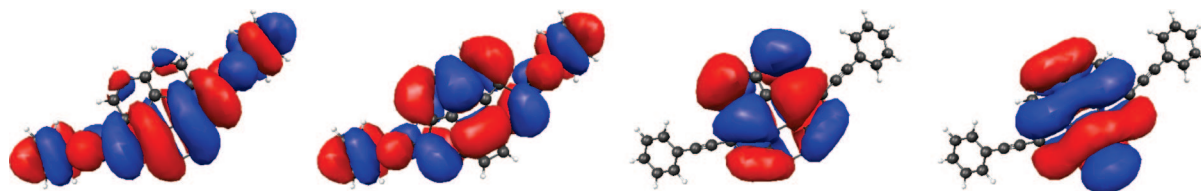


Figure 8. HOMO to HOMO-3 (left to right) for **3-Ph₂**. HOMO and HOMO-1 represent antibonding core-to-field interactions, while HOMO-2 and HOMO-3 are effectively degenerate core orbitals.

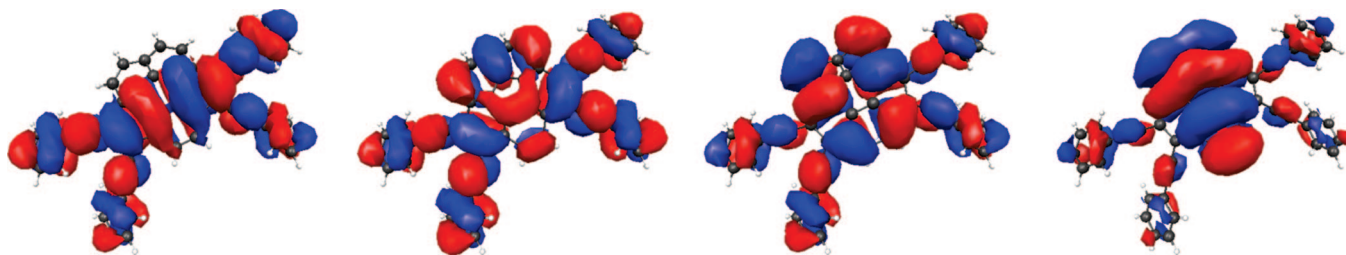


Figure 9. HOMO to HOMO-3 (left to right) for **4-Ph₄**. All represent antibonding core-to-field interactions.



Figure 10. HOMOs of **3-Ph₂**, **14**, and **4-Ph₄** (left to right). All have a common nodal number and structure.

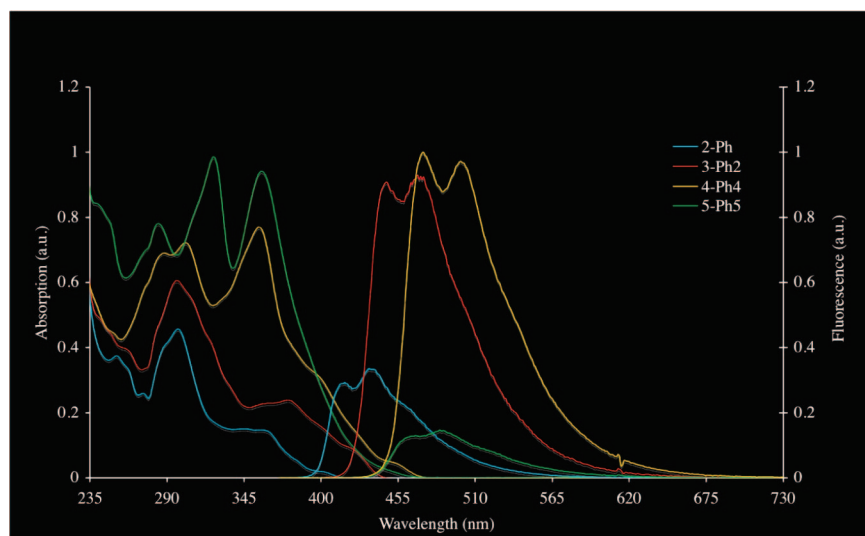


Figure 11. Absorption and emission spectra of the phenylethynyl corannulenes **2-Ph**, **3-Ph₂**, **4-Ph₄**, and **5-Ph₅**.

This extremely simplified model leads one to presume a similarity in character between compounds of classes **2** and **3** and those of mono- and disubstituted fluorenes or biphenyls, which are important chromophores in OLED materials. Indeed, the orbital structure and photophysical behavior of **13** relative to those of **14** serve as a good analogue for the behavior of **2-Ph** relative to **3-Ph₂**.²³ The HOMOs of **3-Ph₂**, **14**, and **4-Ph₄** show a common orbital density and phase pattern (Figure 10). This similarity naturally raises the question of whether these compounds exhibit similar fluorescence behavior.

Computational work on the details of corannulene fluorescence is still ongoing, but we can present here some general empirical trends extracted from the compilation of experimental fluorescence spectra, quantum yields and lifetimes in Table 4. In general, having more substituents leads to longer emission wavelengths (λ_f), with classes **4** and **5** showing the longest λ_f .

(23) Birckner, E.; Grummt, U.-W.; Göller, A. H.; Pautzsch, T.; Egbe, D. A. M.; Al-Higari, M.; Klemm, E. *J. Phys. Chem. A* **2001**, *105*, 10307–10315.

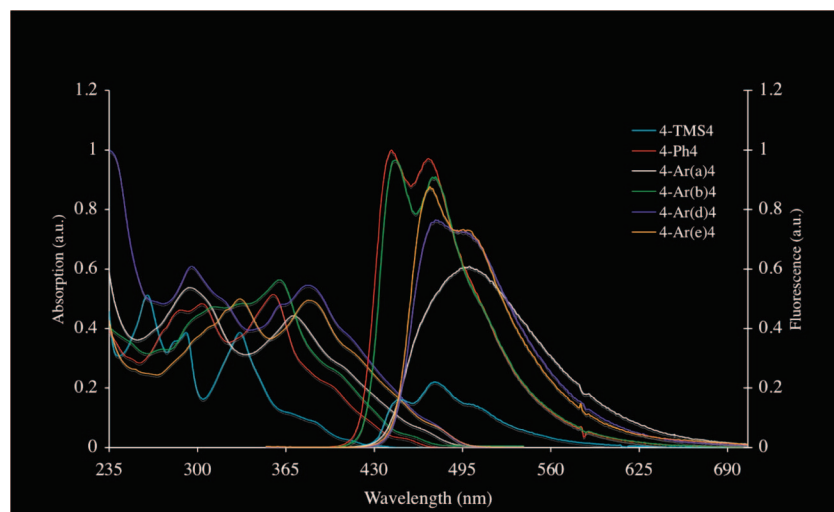


Figure 12. Absorption and emission spectra of the 1,2,5,6-tetraethynyl-substituted corannulenes **4-R₄**.

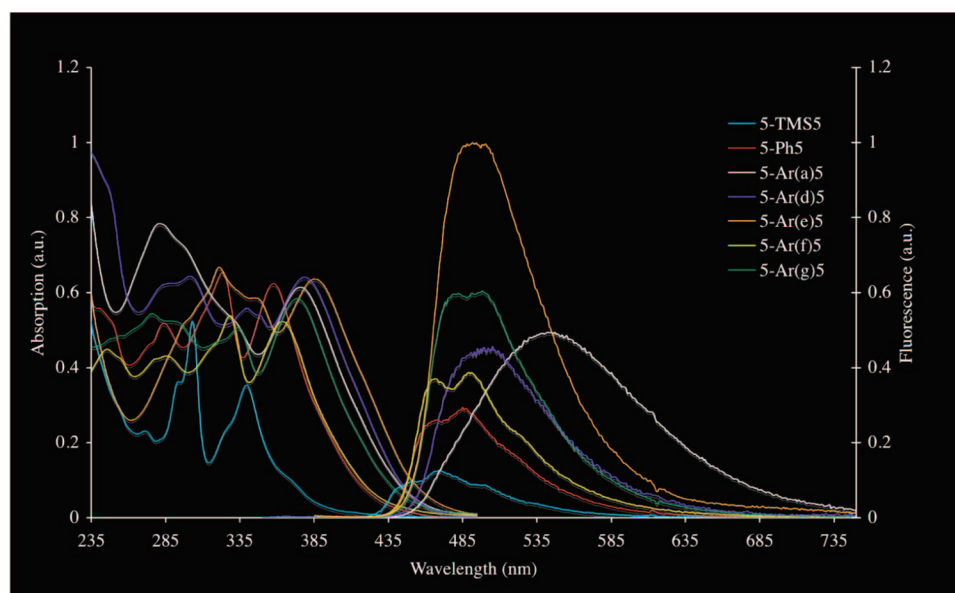


Figure 13. Absorption and emission spectra of the 1,3,5,7,9-pentaethynyl-substituted corannulenes **5-R₅**.

for a given aryl type. The Stokes shifts for the series **2-Ph**, **3-Ph₂**, **4-Ph₄**, and **5-Ph₅** increase slightly (by 40, 45, and 50 nm) for the first three but then jump significantly (> 100+) for the last; a possible explanation for this might be that the emission from **5-Ph₅** is coming from the reverse of the HOMO–LUMO state, which is effectively blocked to absorption by a poor transition moment. A change in the molecular geometry of the excited state could result in better overlap between the states.

The lifetimes (τ) for the series **2-Ph**, **3-Ph₂**, **4-Ph₄**, and **5-Ph₅** are in the range 5–10 ns, with specific values 6.6, 4.8, 10.3, and 10.5 ns, respectively; all of these are a factor of 10 longer than for the model compounds **13** and **14**. The fluorescence quantum yields (Φ_f) for the series **2-Ph**, **3-Ph₂**, **4-Ph₄**, and **5-Ph₅** vary from modest values of 20 and 12% (for **2-Ph** and **5-Ph₅**, respectively) to respectable values of 75 and 83% (for **3-Ph₂** and **4-Ph₄**, respectively). The high quantum yields for **3-Ph₂** and **4-Ph₄** parallel the virtually quantitative yield observed for **14**. A contrast between **2-Ph** and **13** is observed. The modest value for **2-Ph** parallels more closely the behavior of 3-phenethynylphenanthroline, which has been presumed to suffer

quenching due to an activated process and/or intersystem crossing. This supposition was supported by the observation of phosphorescence of 3-phenethynylphenanthroline at low temperature. Preliminary low-temperature work on **2-Ph** hints at similar phosphorescence behavior, but additional work is required before we can ascertain the cause of the low quantum yield at room temperature.

The low quantum yield of **5-Ph₅** is somewhat surprising. There are conflicting reports in the literature regarding the effect of symmetry on quantum yield. A study by Nizhegorodov²⁴ described an increase in quantum yield with symmetry due to an increase in radiative states. More commonly cited is the Ham effect,²⁵ in which high symmetry leads to forbidden transitions between the ground and excited states, as is observed in benzene. Vibrational, environmental, or substitutional perturbation of the molecular symmetry allows previously forbidden states to be accessed and thereby increases absorption and emission properties.²⁶

(24) Nizhegorodov, N. I. *Zh. Prikl. Spektrosk.* **1992**, 57, 477–483.

The study most closely paralleling the situation in **5-Ph₅** describes an increase in quantum yield upon desymmetrization of a carbon-based nanotube.²⁷ This would correctly predict that in the present case, the lower-symmetry molecules **3-Ph₂** and **4-Ph₄** should lead to materials with higher quantum yields. Furthermore, since the lifetimes of **4-Ph₄** and **5-Ph₅** are essentially identical, the lifetime of the fluorescence state is not the differentiating factor. One hypothesis would be that the symmetry of the ground state of **5-Ph₅** allows for various nonradiative relaxation modes and thus results in a lower quantum yield by virtue of an increased rate of nonradiative decay.

More than symmetry must be at play in the quantum-yield behavior of corannulene derivatives. Although the low quantum yield (7%) for the parent, corannulene, seems consistent with the symmetry picture, the value for the lower-symmetry molecule cyclopentacorannulene (1%) reported by Warner and co-workers^{3c} does not. One supposition is that bowl depth and its relation to bowl strain is another factor. Warner and co-workers noted that the radiative decay of cyclopentacorannulene is slower than that of corannulene and hypothesized that this could result from greater strain and/or loss of oscillator strength due to greater out-of-plane bowl distortion. There appear to be many interesting and tunable aspects to the photophysical properties of corannulene derivatives. Clearly, if corannulene-based materials are to find their way into photonic applications, an even better understanding of their photophysical behavior is needed.

Direct comparison of the experimental absorption and emission spectra (Figures 11–13) reveals their complex nature. The details for the series **2-Ph**, **3-Ph₂**, **4-Ph₄**, and **5-Ph₅** have been discussed above. Here it suffices to say that the emission spectra (Figure 11) show that **4-Ph₄** has the longest-wavelength emission; the drop in quantum yield can also be assessed qualitatively from the picture. Among the **4-R₄** series, **4-Ar(a)₄**, whose arene is the electron-rich tris(dodecyloxy)phenyl group, shows the longest emission (Figure 12); this behavior is characteristic of the occurrence of some electron transfer from the arylalkynyl field to the corannulene core. If one follows the derivatives as a function of electron-rich character of the arene, the series reorganizes to **4-Ar(b) < 4-Ph < 4-Ar(e) < 4-Ar(d) < 4-Ar(a)**, and the least-electron-rich compounds show the greatest amount of spectral structure and the shortest Stokes shifts. Thus, the emission wavelength in series **4** appears to be tunable within a modest range. In series **5**, the trend tends to be the same (Figure 13), but all of the quantum yields are somewhat smaller, as explained above.

Conclusion

Here we have provided simple ways to prepare multiethynyl-substituted corannulenes from halo precursors in good-to-excellent yields. These alkynyl derivatives pack in the crystal as columnar stacks and in some cases display polar unit cells. The high fluorescence quantum yields seen for these derivatives demonstrate

their potential utility as photophysically active materials. This combination of materials properties bodes well for the development of photoactive and/or polar liquid-crystalline materials based on substituted corannulenes of high symmetry.

Theoretical Section

The conformational analyses of the molecular systems described in this study, including structural and orbital arrangements as well as property calculations, were carried out using the Gaussian 98²⁸ and GAMESS²⁹ software packages. Structural computations on all of the compounds were performed using hybrid DFT (HDFT) methods. The HDFT method employed Becke's three-parameter functional³⁰ in combination with nonlocal correlation provided by the Lee–Yang–Parr expression^{31,32} including both local and nonlocal terms (B3LYP) as well as the new M06-2X functional of Zhao and Truhlar.³³ Dunning's correlation-consistent cc-pVDZ basis set, which is a [3s2p1d] contraction of a (9s4p1d) primitive set, and the double- ζ polarized sets denoted DZ(2d,p) and DZ+(2d,p), were also employed.³⁴ Full geometry optimizations were performed and uniquely characterized via second-derivative (Hessian) analysis in order to determine the number of imaginary frequencies (0 = minimum; 1 = transition state). From the fully optimized structures, single-point energy computations were performed using the MP2³⁵ dynamic correlation treatment; these provided more accurate energy barriers as well as single-point time-dependent absorption characteristics.³⁶ These levels of theory have previously been shown to be reliable for structural and energetic determinations in these types of compounds. ZINDO computations³⁹ were carried out for comparative purposes. Molecular orbital contour plots used as an aid in the analysis of the results were generated and depicted using the programs 3D-PLTORB³⁷ and QMView.³⁸

Acknowledgment. This work was supported by Swiss National Science Foundation grants to K.K.B. and J.S.S. We are grateful to Don Truhlar for granting us access to the use of the M06-2X functional and computational time on the facilities of the Minnesota Supercomputing Institute.

Supporting Information Available: Complete experimental procedures for preparing all of the compounds and intermediates mentioned in this work, complete ref 28, and crystal structure data in CIF format for **8**, **3-Ph₂**, **4-Ar(c)₄**, and **5-Ar(c)₅**. This material is available free of charge via the Internet at <http://pubs.acs.org>.

JA802334N

(25) Ham, J. S. *J. Chem. Phys.* **1953**, *21*, 756.

(26) (a) Nakajima, A. *Bull. Chem. Soc. Jpn.* **1971**, *44*, 3272–3277. (b) Dong, D. C.; Winnik, M. A. *Photochem. Photobiol.* **1982**, *35*, 17–21.

(27) (a) Shavar, J.; Kono, J.; Portugall, O.; Krstic, V.; Rikken, G. L. J. A.; Miyauchi, Y.; Maruyama, S.; Perebeinos, V. *Nano Lett.* **2007**, *7*, 1851–1855. (b) Sun, Y.-P. *Supramol. Photochem.* **1997**, *1*, 325–390.

(28) Frisch, M. J. Gaussian 98, revision A.6; Gaussian, Inc.: Pittsburgh, PA, 1998.

(29) Schmidt, M. W.; Baldridge, K. K.; Boatz, J. A.; Elbert, S. T.; Gordon, M. S.; Jensen, J. H.; Koseki, S.; Matsunaga, N.; Nguyen, K. A.; Su, S.; Windus, T. L.; Elbert, S. T. *J. Comput. Chem.* **1993**, *14*, 1347–1363.

(30) Becke, A. D. *J. Chem. Phys.* **1993**, *98*, 5648–5652.

(31) Lee, C.; Yang, W.; Parr, R. G. *Phys. Rev. B* **1988**, *37*, 785–789.

(32) Miehlich, B.; Savin, A.; Stoll, H.; Preuss, H. *Chem. Phys. Lett.* **1989**, *157*, 200–206.

(33) Zhao, Y.; Truhlar, D. G. *Theor. Chem. Acc.* **2008**, *120*, 215–241.

(34) Dunning, T. H. *J. Chem. Phys.* **1989**, *90*, 1007–1023.

(35) Moller, C.; Plesset, M. S. *Phys. Rev.* **1934**, *46*, 618–622.

(36) Stratmann, R. E.; Scuseria, G. E.; Frisch, M. J. *J. Chem. Phys.* **1998**, *109*, 8218–8224.

(37) 3D-PLTORB, 3D version; San Diego, 1997.

(38) Baldridge, K. K.; Greenberg, J. P. *J. Mol. Graphics* **1995**, *13*, 63–66.

(39) Bacon, A. D.; Zerner, M. C. *Theor. Chim. Acta* **1979**, *53*, 21–54.